Treatment Strategy With Gene Editing for Late-Onset Retinal Degeneration Caused by a Founder Variant in *C1QTNF5*

Randa T. H. Li,[1,2] Alejandro J. Roman,[3] Alexander Sumaroka,[3] Chloe M. Stanton,[4] Malgorzata Swider,[3] Alexandra V. Garafalo,[3] Elise Heon,[5] Ajoy Vincent,[5] Alan F. Wright,[4] Roly Megaw,[2,4] Tomas S. Aleman,[3] Andrew C. Browning,[6] Baljean Dhillon,[1,2] and Artur V. Cideciyan[3]

[1]Centre for Clinical Brain Sciences, School of Clinical Sciences, University of Edinburgh, Edinburgh, Scotland, United Kingdom
[2]Princess Alexandra Eye Pavilion, NHS Lothian, Edinburgh, Scotland, United Kingdom
[3]Center for Hereditary Retinal Degenerations, Scheie Eye Institute, Department of Ophthalmology, Perelman School of Medicine, University of Pennsylvania, Philadelphia, Pennsylvania, United States
[4]Medical Research Council Human Genetics Unit, Institute of Genetics and Cancer, University of Edinburgh, Edinburgh, United Kingdom
[5]Department of Ophthalmology and Vision Sciences, The Hospital for Sick Children, University of Toronto, Toronto, Ontario, Canada
[6]Newcastle Eye Centre, Royal Victoria Infirmary, Newcastle Upon Tyne, United Kingdom

Correspondence: Artur V. Cideciyan, Center for Hereditary Retinal Degenerations, Scheie Eye Institute, Department of Ophthalmology, Perelman School of Medicine, University of Pennsylvania, 51 North 39th Street, Philadelphia, PA 19104, USA;
artur.cideciyan@pennmedicine.upenn.edu.

RTHL, AJR, and AS are joint first authors.

Received: October 2, 2023
Accepted: November 28, 2023
Published: December 22, 2023

Citation: Li RTH, Roman AJ, Sumaroka A, et al. Treatment strategy with gene editing for late-onset retinal degeneration caused by a founder variant in *C1QTNF5*. *Invest Ophthalmol Vis Sci.* 2023;64(15):33.
https://doi.org/10.1167/iovs.64.15.33

Purpose. Genome editing is an emerging group of technologies with the potential to ameliorate dominant, monogenic human diseases such as late-onset retinal degeneration (L-ORD). The goal of this study was to identify disease stages and retinal locations optimal for evaluating the efficacy of a future genome editing trial.

Methods. Twenty five L-ORD patients (age range, 33–77 years; median age, 59 years) harboring the founder variant S163R in *C1QTNF5* were enrolled from three centers in the United Kingdom and United States. Patients were examined with widefield optical coherence tomography (OCT) and chromatic perimetry under dark-adapted and light-adapted conditions to derive phenomaps of retinal disease. Results were analyzed with a model of a shared natural history of a single delayed exponential across all subjects and all retinal locations.

Results. Critical age for the initiation of photoreceptor loss ranged from 48 years at the temporal paramacular retina to 74 years at the inferior midperipheral retina. Subretinal deposits (sRET-Ds) became more prevalent as critical age was approached. Subretinal pigment epithelial deposits (sRPE-Ds) were detectable in the youngest patients showing no other structural or functional abnormalities at the retina. The sRPE-D thickness continuously increased, reaching 25 µm in the extrafoveal retina and 19 µm in the fovea at critical age. Loss of light sensitivity preceded shortening of outer segments and loss of photoreceptors by more than a decade.

Conclusions. Retinal regions providing an ideal treatment window exist across all severity stages of L-ORD.

Keywords: retinal degeneration, basal linear deposits, subretinal space, natural history

Late-onset retinal degeneration (L-ORD) is an autosomal dominant blindness caused by variants in *C1QTNF5* (also known as *CTRP5*), a member of the complement 1q gene family.[1–6] *C1QTNF5* encodes a secreted membrane–associated protein expressed in the retinal pigment epithelium (RPE) and ciliary body epithelium in the eye.[3,7–9] Since the original discovery of a c.489C>G substitution (resulting in a S163R variant) in *C1QTNF5* causing L-ORD, six other disease-causing variants have been found associated with L-ORD: P186S, P188T, P188L, S190W, G216C, and a distinct S163R variant resulting from a c.489C>A substitution.[6,10–12] A seventh variant, Q180E, could also be associated with retinal disease that appears to have a different phenotype compared to L-ORD.[13]

L-ORD is a rare disease, but its prevalence can be relatively higher in some ethnicities or geographies. Most L-ORD patients carry the c.489C>G substitution, which is thought to be a founder variant, arising in southeast Scotland and spreading into England and across to Canada and the United States in the early 1800s.[1–6,14–17] Patients with

L-ORD have an asymptomatic stage typically for the first four decades of life, followed by a symptomatic stage with night blindness and characteristic retinal changes (typically between the ages of 40 and 60 years). Later stages can include reduced visual acuity, patchy retinal atrophy, and neovascularization.[1,18] Despite mechanism-confirming interventions with high-dose vitamin A[2,14] and in vitro amelioration of the cellular phenotype with gene augmentation or with metformin,[19] L-ORD remains without treatment.

The c.489C>G substitution in *C1QTNF5* is particularly suitable for treatment with gene editing. First, the retina, in general, is a highly accessible organ for therapeutic delivery; its structure can be easily imaged and visual function easily assessed. Second, the c.489C>G variant is the most prevalent cause for L-ORD; thus, a variant-specific therapy would be applicable to many families in Europe and North America. Third, the c.489C>G variant is thought to cause dominant-negative disease,[6] which necessitates an approach targeting the mutant allele, such as knockdown/replacement gene therapy[20] or gene correction.[21] Fourth, the c.489C>G mutation introduces a novel protospacer adjacent motif (PAM) site, allowing for specific targeting of only the mutant allele. Finally, the protein is expressed in the RPE, which is relatively easier to transfect with viral vectors as compared to other retinal cell types.[22]

L-ORD was initially discovered and named based on histopathologic examination of an eye donor showing thick sub-RPE deposits (sRPE-Ds) located between the basal lamina of the RPE and the inner collagenous layer of Bruch's membrane (BrM).[1,3,23,24] These deposits resemble the basal linear deposits found in age-related macular degeneration (AMD). In addition, L-ORD shares other clinical features with AMD, such as subretinal deposits (sRET-Ds), also known as subretinal drusenoid deposits or reticular pseudodrusen,[17,25–28] retinal atrophy, and choroidal neovascularization. Several characteristics distinguish L-ORD from AMD, including a strong family history of visual impairment, extensive extramacular atrophy often preceding foveal loss, and the presence of long anterior zonules visible further centrally on the anterior lens capsule.

Subcellular features in the outer retina of patients with L-ORD can now be quantified in vivo using non-invasive imaging.[4] In preparation for a gene editing clinical trial, we therefore evaluated a large cohort of patients carrying the c.489C>G variant to generate quantitative phenomaps consisting of photoreceptor nuclear and outer segment thicknesses, sRET-D and sRPE-D thicknesses, and colocalized light sensitivities mediated by rods and cones. The phenomaps were analyzed in patients across five decades to infer the underlying natural history of this specific molecular form of L-ORD and predict retinal locations and patient ages that may be amenable to gene editing.

Methods

Subjects

Twenty-five patients (15 female) who were molecularly confirmed as heterozygous for the c.489C>G variant in *C1QTNF5* were included in this study (Table). Ages of patients ranged from 33 to 77 years (median, 59 years). Patients P002, P003, and P006 are direct descendants of the eye donor[1] that defined L-ORD. Evaluations at earlier ages have been reported in 10 of 25 patients[1–4,15] (Table). Patients

Table. Patient Demographics

ID	Age (y)	Sex	VA (logMAR)		SE Refraction (D)		sRET-D	Family Relationship and Previous Publication
			RE	LE	RE	LE		
E009	33	F	−0.22	−0.20	0.00	0.50	N	Child of E001
N004	40	F	−0.14	−0.20	1.00	0.50	N	—
E010	42	M	−0.20	−0.20	0.00	0.00	N	Child of patient VI-8 from Family 1 in Jacobson et al.[2]
E013	43	F	−0.08	−0.12	−1.00	−0.75	Y	Child of E014
P002	48	F	−0.14	−0.10	−0.50	−1.00	N	Child of P003
P005	49	F	−0.04	−0.04	−4.75	−4.50	Y	Patient III-4 in Vincent et al.[15]
N001	51	F	−0.10	−0.06	1.25	2.00	Y	Related to E017
N006	52	F	−0.10	−0.06	0.00	0.00	Y	Sibling of N009
N009	54	M	−0.06	−0.14	−0.25	−0.25	Y	Sibling of N006
N005	56	F	−0.14	−0.08	−0.50	−1.75	Y	—
N003	58	F	0.04	0.04	0.00	0.25	Y	—
E006	59	F	0.00	−0.10	1.50	1.00	Y	Patient VII-4 from Family 1 in Jacobson et al.[2]
E003	59	F	0.00	0.00	1.75	1.50	Y	Patient VII-5 from Family 1 in Jacobson et al.[2]
E004	62	M	0.00	0.00	−2.00	−2.50	Y	Patient VII-3 from Family 1 in Jacobson et al.[2]
N002	63	M	0.06	0.08	−1.50	−0.25	Y	—
E008	64	F	0.00	0.00	0.00	1.00	Y	Patient VII-2 from Family 1 in Jacobson et al.[2]
E014	65	M	0.00	0.10	−0.50	−1.50	Y	—
E001	66	M	1.30	1.30	−4.50	−3.75	N	Patient VII-1 from Family 1 in Jacobson et al.[2]
N010	66	F	0.02	−0.08	2.75	2.50	Y	—
E002	68	M	1.28	1.26	1.25	1.25	—	Patient III-7 from Family L8 in Hayward et al.[3]
E017	68	F	3.00*	3.00*	1.50	1.25	—	Related to N001
E011	69	M	0.12	0.00	0.25	−0.25	—	—
P001	74	M	2.00	1.60	6.00	6.00	—	Patient II-4 in Vincent et al.[15]
P006	75	M	1.70	0.64	0.00	0.00	—	Patient IV-1 in Kuntz et al.[1]
P003	77	F	1.58	1.22	−2.00	1.00	—	Patient 2 in Jacobson et al.[4]; child of Patient III-3 in Kuntz et al.[1]

VA, visual acuity; SE, spherical equivalent; RE, right eye; LE, left eye; sRET-D, subretinal deposit; F, female; M, male; N, no; Y, yes.
*Hand motions (HM) assigned to 3.0 logMAR.

were enrolled at three clinical sites: Princess Alexandra Eye Pavilion, NHS Lothian, Edinburgh, Scotland, UK; the Newcastle Eye Centre, Royal Victoria Infirmary, Newcastle Upon Tyne, UK; and, the Center for Hereditary Retinal Degenerations (CHRD), Scheie Eye Institute, University of Pennsylvania, Philadelphia, USA.

Ethics

This study adhered to the tenets of the Declaration of Helsinki and was approved by the institutional review boards of the three clinical sites where patients were enrolled. Written informed consent was obtained from all participants prior to participation in the study.

Clinical, Imaging, and Functional Evaluations

Patients underwent complete eye examinations, best-corrected visual acuity measurements, and several ancillary tests. En face imaging was performed with a confocal scanning laser ophthalmoscope (SPECTRALIS HRA; Heidelberg Engineering, Heidelberg, Germany) using the 55° lens in two modes: reflectance imaging with near-infrared illumination (NIR-REF) and autofluorescence imaging with short-wavelength excitation (SW-AF). The dilated pupil of the subject was aligned with the optical axis of the instrument, and images obtained were centered on the anatomical fovea. The manufacturer's automatic real time (ART) feature was used to obtain averaging to increase the signal-to-noise ratio.

Optical coherence tomography (OCT) imaging was performed with a SPECTRALIS spectral-domain system. The acquisition protocol used a 30° lens and six overlapping 30°-long high-resolution line scans (ART = 20). Three of the scans were along the horizontal meridian, and three were along the vertical meridian. Each set of three scans included one scan where the fovea was centered and two scans where the fovea was near the start or end of the scan, respectively. Post-acquisition data analysis was performed with custom programs (MATLAB; MathWorks, Natick, MA, USA) as previously described.[4,29,30] Individual scans were digitally stitched to create widefield (~55°) OCT images centered on the fovea along the horizontal and vertical meridians, straightened, and resampled by averaging 25 neighboring a-scans. For quantitative analyses, the hyposcattering outer nuclear layer (ONL) was defined between the hyperscattering layer attributed to the outer plexiform layer (OPL) and the hyperscattering outer limiting membrane (OLM) and included the anatomic layers of both ONL and Henle's fiber layer. Directional OCT images that distinguish between ONL and Henle's fiber layer[31] were not available. For outer retinal sublaminae, the four major sublaminae considered were (1) inner segment (IS)/outer segment (OS), a hyper-reflective layer near the junction of inner and outer segments; (2) ROST, a hyper-reflective layer near the interface between rod outer segments tips (ROSTs) and RPE apical processes; (3) RPE, a hyper-reflective layer originating from the RPE; and (4) BrM, Bruch's membrane (Supplementary Fig. S1). In normal subjects, ROST, RPE, and BrM peaks were always amalgamated into a single larger peak. Within the macula but outside of the fovea, there was also consideration of a hyper-reflective layer originating near the interface between cone outer segment tips (COSTs) and RPE apical processes. Outside the macula, COST was either not detectable or merged into IS/OS. At the fovea, COST and ROST peaks could merge.

Chromatic static perimetry was performed with a computerized perimeter (MonCVOne; Metrovision, Pérenchies, France) using methods similar to those previously described.[30,32–35] Light-adapted (600 nm) and two-color (500 and 650 nm) dark-adapted function was measured at 2° intervals across the visual field extending to 30° from the fixation along horizontal and vertical meridians. Considering the slow kinetics of dark adaptation, bright lights (such as autofluorescence imaging, fundus photography, or fundus exams) were avoided during the period preceding dark-adapted testing. Both eyes were dark adapted for a period of at least 45 minutes. Right eyes were tested first and left eyes second; due to the duration of dark-adapted testing in the first tested right eye, the left eyes received a longer duration of dark adaptation. Available evidence was consistent with the idea that full dark-adapted function was achieved in both eyes within the current protocol; however, to err on the safe side, only results from left eyes were analyzed and presented. Photoreceptor mediation under dark-adapted conditions was determined by the sensitivity difference between the 500- and 650-nm stimuli.

Statistics

To understand the natural history of disease, a delayed exponential time course was assumed to underlie progression of photoreceptor degeneration and light sensitivity loss as a function of time. As previously described,[36–41] such modeling describes a natural history consisting of an initial period of no change, followed by exponential progression. Both structural dependent variables (ONL and ROS thickness measured in micrometers) were first divided by retinal locus-specific normal values and then logarithmically transformed. Both functional dependent variables (rod and cone sensitivity measured in logarithm) were specified after subtraction from locus-specific normal values. The relationship between the logarithm of the ONL fraction and time was first evaluated with an ensemble model consisting of a first segment of zero intercept and zero slope followed by a second segment starting at the breakpoint time and having a negative slope. Time was the chronological age of each patient, and variables were breakpoints corresponding to the 45 sampled retinal loci and a single common slope representing the rate of progression across all locations. Minimizing the squared error terms produced the best estimates for the model variables. Locus-specific breakpoints from this ensemble model represented the critical age for the inferred start of ONL thinning and thus initiation of retinal degeneration. Next, time from critical age was calculated by subtracting chronological age from the critical age for each patient and each retinal locus. Individual models examined each dependent variable (rod and cone sensitivities and logarithms of ONL and ROS fractions) pooled across the retina as a function of time from critical age, with a delayed exponential model having first-segment slope and intercept fixed to zero and allowing a single breakpoint time and a single second-segment slope to vary. Modeling was performed using the L-BFGS-B method[42] of the optimx package v.2022.04.30[43] in R 4.1.3 (R Foundation for Statistical Computing, Vienna, Austria).

Results

Patients with L-ORD show a progressive retinal disease that is clinically detectable in the sixth and seventh decades of

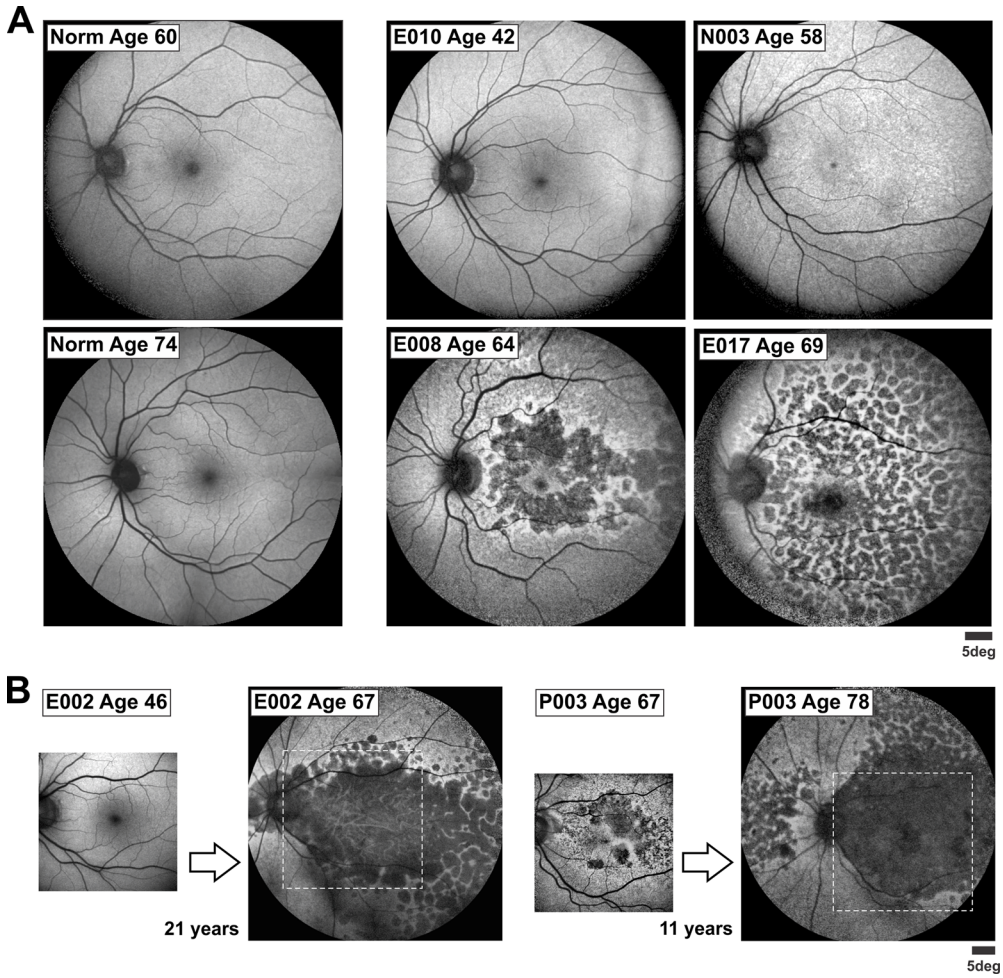

Figure 1. Short-wavelength autofluorescence (SW-AF) imaging can map L-ORD disease progression. (**A**) SW-AF identifies the spatial distribution of RPE health by providing a signal related to the lipofuscin content of cells across the retina. Images of four L-ORD patients, representing different stages of disease, are compared to two healthy (Norm) subjects. Brighter areas of hyperautofluorescence represent stressed RPE, and darker areas of hypoautofluorescence represent RPE atrophy. (**B**) Long-term follow up in two L-ORD patients. E002 showed development of large areas of atrophy from normal retina over 21 years. P003 showed substantial expansion of areas of atrophy over 11 years. *Dashed squares* at later visits show the smaller area imaged at earlier visits. Image contrasts are stretched to improve the visibility of structures. *Calibration bars* are shown.

life, and SW-AF can provide a coarse staging of RPE disease as demonstrated by several representative examples (Fig. 1). E010 at age 42 was not symptomatic and correspondingly showed normal-appearing SW-AF images, whereas N003 at age 58 had symptoms of nyctalopia and showed disturbances on SW-AF imaging without obvious RPE atrophy (Fig. 1A, upper row). Later stages of L-ORD with more severe vision loss are represented by E008 and E017 (Fig. 1A, lower row). E008 at age 64 demonstrated areas of atrophy in the macula and temporal retina; visual acuity (Table) and the foveal region were preserved. E017 at age 69 had larger areas of macular and paramacular atrophy with severe loss of visual acuity (Table).

Within any one individual, progression tends to be slow, and detection of major changes before the onset of RPE atrophy requires long-term follow-up. After the onset, there is progressive expansion of areas of atrophy.[27] Two rare examples with serial follow-up performed over more than a decade exemplify the onset and expansion of atrophy (Fig. 1B). Patient E002 demonstrated no RPE abnormalities at age 46 but subsequently developed large regions of RPE atrophy by age 67. Patient P003 exhibited scattered parafoveal and perifoveal abnormalities at age 67 that grew substantially in extent and severity by age 78 (Fig. 1B).

Outer Retinal Structures Apparent on OCT in L-ORD

To evaluate outer retinal changes, widefield OCT imaging was used to cover a 55°-diameter region along horizontal and vertical cardinal meridians in the current cohort of 25 patients (Table). Comparison of OCTs between healthy and L-ORD eyes at the cusp of the sixth decade of life demonstrated representative examples of early disease features along the vertical meridian (Supplementary Fig. S1). Qualitatively, L-ORD patients showed retained outer retinal layers with mild disturbances including spatially heterogeneous sRET-Ds in the inferior retina of E006 and local parafoveal disorganization of the OS layer in E004 (Supplementary Fig. S1A, white diagonal arrows). Notable was the distinct separation of BrM from the RPE with the introduction of a hyposcattering layer in both L-ORD patients (Supplementary Fig. S1A).

Quantitation of OCTs along the full extent of meridians provided data to build phenomaps in L-ORD. Two superior retinal locations, centered at 12 and 23 degrees of eccentricity from the fovea, helped define the structures measured (Supplementary Fig. S1B). In the outer retina of healthy eyes, the inner hyperscattering peak is thought to originate near the junction between the inner and outer segments (IS/OS), whereas the outer hyperscattering peak likely has contributions from rod outer segment tips, RPE pigments, and BrM (ROST/RPE/BrM). Higher axial resolution equipment can often differentiate between these latter peaks[29,44]; however, with the equipment used in the current study, the subpeaks were mostly merged into a single peak in healthy eyes. In L-ORD eyes, RPE and BrM peaks were separated by sRPE-Ds (Supplementary Fig. S1B, *) and ROST and RPE peaks were separated by sRET-D (Supplementary Fig. S1B, +). At retinal locations with retained photoreceptors and RPE, all L-ORD eyes had evidence of sRPE-Ds. All eyes but two within the age range of 43 and 66 showed detectable sRET-Ds at some but not all retinal locations (Table). At locations with retinal atrophy, identification of RPE and sRPE-D was more challenging but possible (Supplementary Fig. S2).

ExtraFoveal Loss of ONL Thickness

A prerequisite for estimating the treatment potential for improving vision with an intervention in L-ORD is the existence of photoreceptor cells remaining in each eye, and the thickness of the ONL can provide this information. ONL thickness variation measured across all eyes showed a complex combination of features involving age and retinal location, as well as other sources of variation (Fig. 2A). To explain some of this complexity, we hypothesized the existence of a natural history of disease wherein measurable photoreceptor degeneration starts at a critical age, after a decades-long delay. When initiated, photoreceptor degeneration progresses exponentially. To a first approximation, we assumed that this basic natural history model is shared across the retina of all patients with L-ORD harboring the c.489C>G variant after allowing for retinal-locus–specific variation of the critical age parameter but keeping the time constant of the exponential decay invariant across the retina. This so-called "delayed exponential" model has been previously used to describe disease progression in humans[36–38,41] and animals.[39,40]

We used cross-sectional ONL thickness data from all patients to estimate the critical age for the initiation of photoreceptor degeneration at each retinal locus. The ensemble best-fit model (Supplementary Figs. S3, S4) had an invariant rate constant of -0.045 $\log_{10}$/y (corresponding to 9.8%/y). Two locations along the vertical meridian demonstrated variation of the critical ages within the retina (Fig. 2A, insets). At 20° inferior to the fovea, the estimated critical age for photoreceptor loss detectable by OCT is 69.3 years, whereas at 4° inferior to the fovea, the critical age is 51.7 years. Our model implies that the natural history of disease progression at 20° duplicates that of the parafoveal locus after a 17.6-year delay, on average, with the same progression rate.

Across the vertical meridian, estimated critical ages ranged from 48.9 to 74 years (Supplementary Fig. S3), whereas across the horizontal meridian the range was from 47.7 to 70.6 years (Supplementary Fig. S4). The locations with the earliest initiation of photoreceptor loss were 6° superior, inferior, and nasal to the fovea and 10° to 20° degrees temporal to the fovea (Fig. 2B). Theoretically, foveal cone losses could affect the parafoveal ONL thickness as measured here due to the eccentric loss of the Henle's fiber layer. However, as described later, L-ORD shows relative preservation of the foveal cones; thus, we estimated the parafoveal ONL thinning to correctly localize to parafoveal photoreceptors.

There was surprising superior–inferior asymmetry in extramacular locations, with inferior retina showing a delay of between 3 and 12 years in reaching critical age as compared to superior retina. Notably, inferior retinal locations beyond 22° had normal or near-normal ONL thickness even in the three oldest patients (Figs. 2A, 2B; Supplementary Figs. S3, S4), reminiscent of the preserved far inferior retina described in end-stage disease.[1]

When normalized by critical age differences across retinal locations, the underlying shared natural history of outer retinal changes could be inferred. Overall, the data covered an ~50-year duration extending from ~30 years before critical age to ~20 years after. A delayed exponential fit to the normalized data had a rate of -0.045 log/y, which was expectedly identical to the ensemble fit. Based on ONL thickness, more than 65% of photoreceptors would be expected to be lost within a decade after critical age (Fig. 2C), implying a relatively short window of intervention to arrest degeneration after it has initiated.

ExtraFoveal Loss of ROS Thickness

For the partially retained photoreceptors to have the capacity to signal light at any stage of disease, the existence of rod outer segments (ROSs), containing rhodopsin, is required. In typical retinal degenerative conditions, ROS length tends to proportionally shorten with ONL thinning.[45] In L-ORD, there is also a tendency for ROS shortening to follow ONL thinning across disease stages (Supplementary Fig. S5). Consistent with that tendency, initiation of ROS shortening occurred near the retinal-locus–specific critical age, on average preceding it by 4.5 years (Fig. 2E). Also consistent was the similarity of the rates of ROS shortening and ONL thinning, with the former being -0.05 $\log_{10}$/y (corresponding to 10.8%/y) (Fig. 2E).

ExtraFoveal Accumulation of SubRetinal Deposits

Although originally not described in histopathological studies,[1,3,23,24] it is now accepted that some L-ORD patients display sRET-Ds at some stages of disease.[26,28] In our cohort, there was a complex relationship between age and detectability of sRET-Ds on OCT imaging (Table). The youngest three patients, between the ages of 33 and 42 years, had no evidence of sRET-Ds. Among the 16 patients between the ages of 43 and 66 years, 88% showed some retinal locations with detectable ROS and detectable sRET-Ds (Table). Among the oldest six patients between the ages of 68 and 77 years, interpretation of sRET-Ds was complicated by the fact that they either did not have detectable ROSs (Supplementary Fig. S2) or showed very small regions with retained ROSs located near the ends of scans, which tended to have lower signal-to-noise ratios.

Locus-by-locus analyses of sRET-Ds across all eyes, normalized by critical age, showed interpretable tendencies across stages of disease progression (Fig. 2D). Between 15 and 30 years preceding critical age, less than 10% of the locations sampled showed detectable sRET-Ds, and the thickness

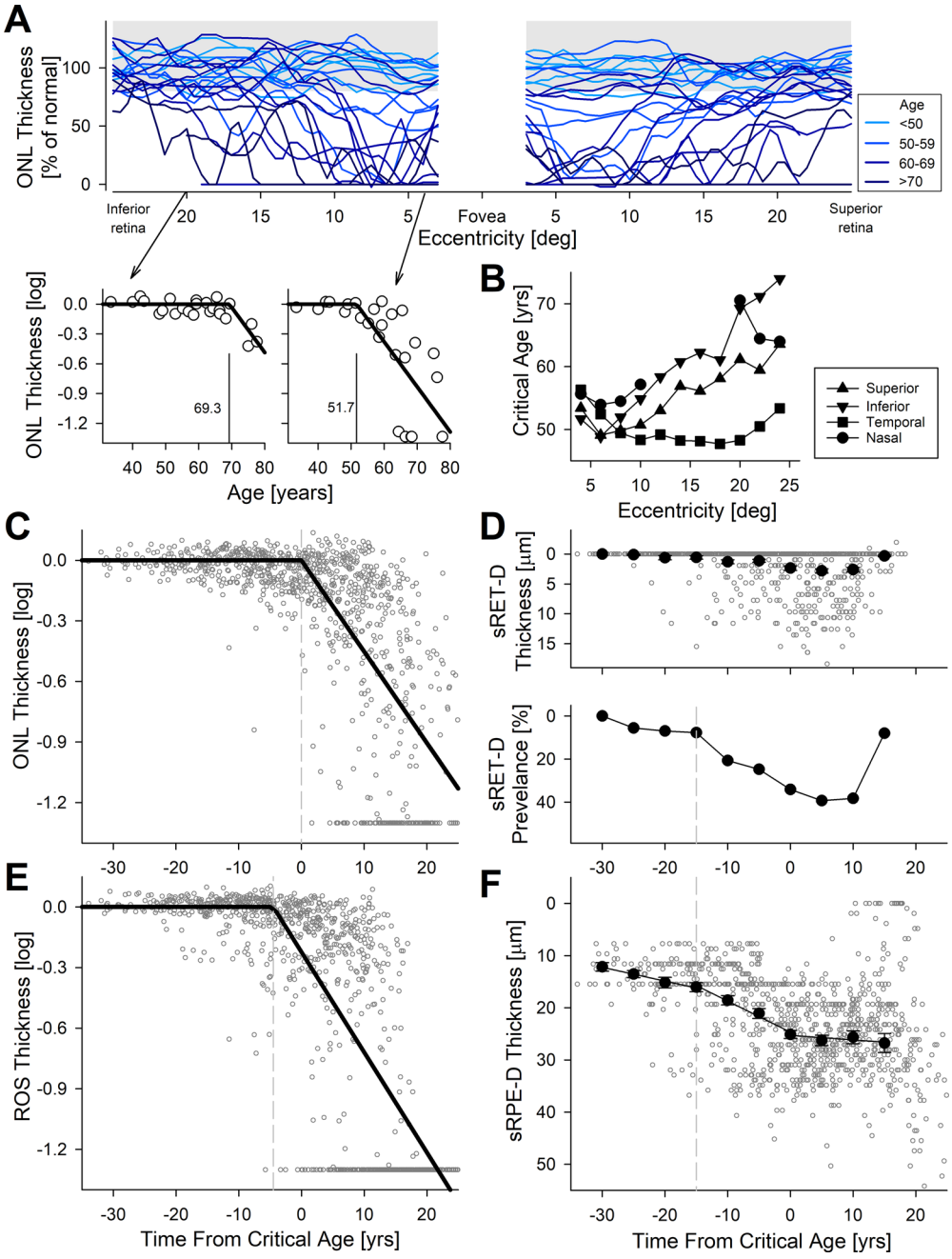

Figure 2. Quantification of outer retinal features in L-ORD identifies predictable variation across the retina across all disease stages. (**A**) ONL thickness (as a percentage of mean normal value at each location) along the vertical meridian shows variation with age and retinal location. All data are from left eyes. Foveal area is plotted separately in Figure 5. (*Insets*) Log ONL thickness as a function of age at two locations in inferior retina, demonstrating variation in critical age (vertical line and numbers) as estimated from a delayed exponential model. All locations are plotted in Supplementary Figures S3 and S4. (**B**) Estimates of critical age as a function of eccentricity along the vertical and horizontal meridians highlight that the loss of ONL temporal to the fovea begins earlier than elsewhere in the retina. Missing data in the nasal retina correspond to the optic nerve. (**C**, **E**) ONL thickness (**C**) and ROS length (**E**) measures pooled across all patients and all locations as a function of time from critical age show rapid degeneration when patients reached critical age at each location. A natural history model best fit to the pooled data is shown (*black line*). *Vertical dashed lines* represent the time when the exponential progression segment of natural history began. (**D**) sRET-D thickness and prevalence as a function of time from critical age. *Symbols* are mean values calculated for 5-year-wide bins. The *vertical dashed line* at −15 years represents the apparent time when the prevalence of the sRET-D began to increase. (**F**) sRPE-D thickness as a function of time from critical age. *Symbols* are mean values calculated for 5-year-wide bins. *Lines* represent three piecewise linear regressions. The *vertical dashed line* at −15 years represents the apparent time when the accumulation rate of sRPE-D began to increase.

Investigative Ophthalmology & Visual Science

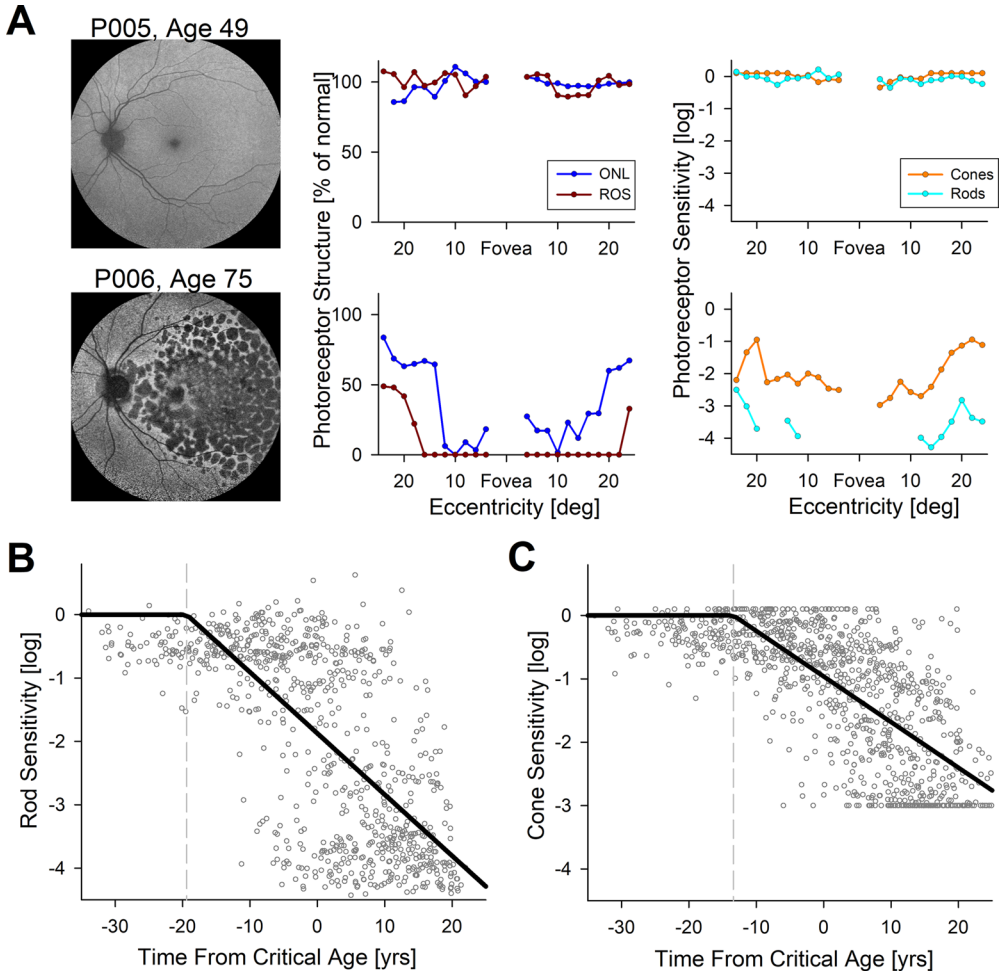

Figure 3. The relationship of rod- and cone-mediated sensitivity as a function of colocalized changes in photoreceptor structure shows early loss of rod sensitivity. (**A**) Profiles of ONL and ROS thickness (*left column*) and rod- and cone-mediated sensitivities (*right column*) of two patients representing different severity stages. Data along the vertical meridian are shown. All thickness and sensitivity data are normalized to retinal-locus–specific mean normal values. (**B**, **C**) Rod (**B**) and cone (**C**) sensitivities pooled across all locations in all patients as a function of critical age show that the loss of rod sensitivity preceded the loss of cone sensitivity, and both sensitivity losses began more than a decade before critical age. A natural history model best fit to the pooled data is shown (*black line*). *Vertical dashed lines* represent the time when the exponential progression segment of the natural history began.

of deposits averaged less than 1 µm due to their low prevalence (Fig. 2D). Starting 15 years before critical age, there appeared to be an increase in the prevalence of sRET-Ds, reaching a peak of near 40% of the locations sampled and a thickness approaching 3 µm, on average, at critical age (Fig. 2D). Beyond 10 years following critical age, there was a return to a low prevalence of sRET-Ds, likely secondary to the lack of detectable ROS structures.

ExtraFoveal Accumulation of sRPE-Ds

The existence of deposits between the RPE and BrM was easily detectable, and sRPE-D thickness was able to be quantified in all patients (Fig. 2F). Surprisingly, even the youngest patient (E009) at age 33 years had clear evidence of sRPE-Ds with thicknesses of 10 to 15 µm (normal sub-RPE space is estimated to be less than 4 µm). Limited clinical data from E009 obtained at age 28 showed that sRPE-D thickness did not change substantially during the 5-year interval (data not shown). Equally surprisingly, at the atrophic stage of disease, some areas appeared to retain remnants of RPE and sRPE-Ds (likely underlying the scalloped atrophy appearance clinically), whereas other areas showed only a BrM signal, with no RPE and no sRPE-Ds (Supplementary Fig. S2). The relation of sRPE-D thickness with critical age appeared to be highly predictable, with continuous lifetime accumulation starting with a mean value of 12-µm deposit thickness 30 years before critical age (Fig. 2F). There were distinct similarities between sRET-D and sRPE-D accumulation trajectories. Specifically, between 15 and 30 years preceding critical age, sRPE-D accumulation rate was shallow, averaging 2.7 µm per decade (Fig. 2F). Starting 15 years before critical age, there was a doubling of the sRPE-D accumulation rate, averaging 6 µm per decade (Fig. 2F). After critical age, there was a flattening of accumulation rate, potentially supporting the hypothesis that some of the sRPE-Ds cleared upon photoreceptor loss (Fig. 2F).

ExtraFoveal Loss of Rod- and Cone-Mediated Sensitivities

To understand the relation between outer retinal structural changes and loss of vision, we sampled light sensitivities

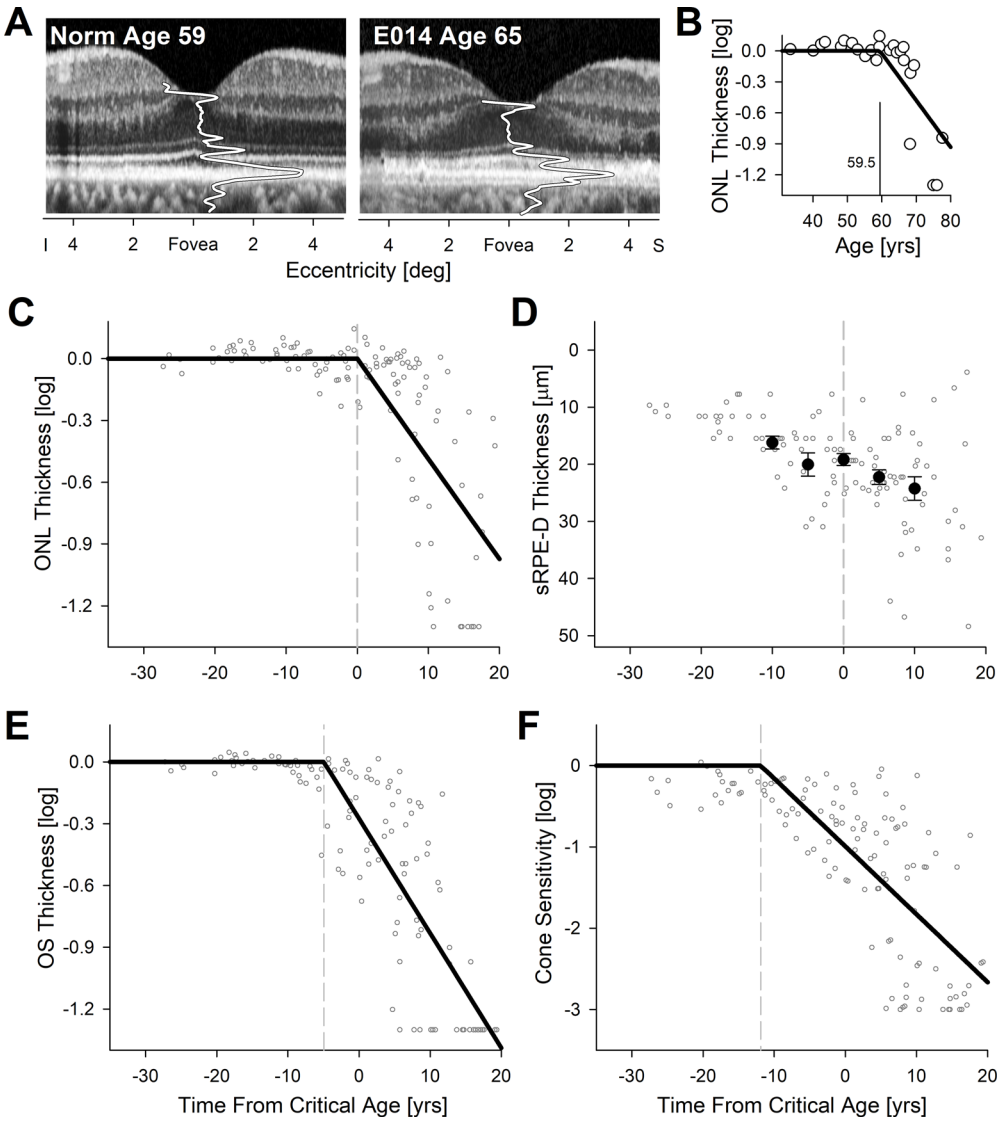

Figure 4. Foveal cone photoreceptor structure and cone-mediated sensitivity. (**A**) Central macular OCTs in a normal subject compared to L-ORD patient E014. Overlaid are the longitudinal reflectivity profiles (*white traces*) at the foveola showing preservation of the outer retinal hyperscattering peaks despite sRPE-Ds. (**B**) Foveolar log ONL thickness as a function of age demonstrating that the critical age (*vertical line* and *number*) is later that that of the perifovea, as estimated from a delayed exponential model. (**C**, **E**) ONL thickness (**C**) and OS length (**E**) in the foveal region (foveola and 2° eccentric) pooled across all patients as a function of time from critical age show that OS loss slightly precedes ONL loss. (**D**) sRPE-D thickness as a function of time from critical age shows accumulation. *Black symbols* are mean values calculated for 5-year-wide bins. (**F**) Cone sensitivity at the foveal region pooled across all patients as a function of critical age. A natural history model best fit to the pooled data is shown (*black lines* in **C**, **E**, and **F**). *Vertical dashed lines* represent the time when the exponential progression segment of the natural history began.

along both principal meridians. We used light-adapted perimetry with orange (600 nm) stimuli to estimate local cone sensitivity and two-color dark-adapted perimetry to estimate local rod sensitivity. At the extremes, light sensitivity was well correlated with photoreceptor structure, as exemplified by two patients. P005 at age 49 years showed a disease stage with a normal ONL thickness and normal ROS thickness throughout the vertical profile (Fig. 3A). Rod and cone photoreceptor sensitivities were also normal throughout (Fig. 3A). In contrast, P006 at age 75 years had severe loss of ONL and ROS layer thickness associated with major abnormalities in rod and cone function (Fig. 3A).

The complexity of functional loss became apparent upon examination of photoreceptor sensitivity as a function of critical age across the retina. In general, light sensitivities driven by rods and by cones were more retained before critical age and substantially abnormal after critical age (Figs. 3B, 3C). However, a delayed exponential fit to the data showed that, on average, loss of rod sensitivity started 19.6 years before critical age (Fig. 3B) when ONL thickness and ROS length were mostly normal (Figs. 2C, 2E). When initiated, the average progression rate of rod sensitivity loss was −0.097 $\log_{10}$/y (corresponding to 20%/y). Loss of cone sensitivity appeared to be less severe, starting 13.4 years before critical age and progressing at −0.07 $\log_{10}$/y (or 14.9%/y) (Fig. 3C).

Foveal Structure and Function

The current cohort of L-ORD patients was consistent with previous publications showing relative retention of visual

acuity even in later stages of disease. Specifically, 17 patients between the ages of 33 and 65 years retained normal visual acuity in both eyes (Table). E014 at age 65 years demonstrated a representative example of the foveal outer retinal structure in L-ORD with retained visual acuity as compared to an age-matched normal subject (Fig. 4A). ONL and OS layers were of normal thickness, with some minor disturbances apparent immediately outside of the foveola. Of note, RPE and BrM peaks were separated by an abnormal hyposcattering layer where sRPE-D thickness can be measured. Among the eight patients older than 66 years, two patients retained normal visual acuity in both eyes, whereas the remaining eyes were worse than 20/200 Snellen equivalent (Table). ONL thickness at the foveola was plotted as a function of age to better understand the natural history of foveal cone photoreceptor loss. The estimated critical age for foveolar cone photoreceptor loss across all patients was 59.5 years (Fig. 4B), which was delayed by about a decade as compared to the critical ages at the perifovea (dominated by rod photoreceptor loss) (Figs. 2A, 2B). When considering the central 5°-diameter foveal region centered on the foveola, cone photoreceptor loss rate was −0.049 $\log_{10}$/y, which was comparable to the rod photoreceptor loss rate (Fig. 4C). Thinning of the foveal OS preceded critical age by 5 years but progressed with a rate comparable to that of the ONL (Fig. 4E). Unlike extrafoveal locations, there was no evidence of sRET-Ds at foveal locations in any of the eyes at any age (data not shown). However, there were definite sRPE-Ds at the fovea in all eyes (Fig. 4D). There were not enough data to reliably estimate the accumulation rate of sRPE-Ds at the fovea, but results at the fovea appeared to be similar to extrafoveal locations (Fig. 2F). Initiation of cone photoreceptor sensitivity losses at the fovea started 11.9 years before the critical age and progressed at −0.084 $\log_{10}$/y (Fig. 4F).

Discussion

Extraordinary progress in molecular medicine achieved over the last decade promises novel treatment strategies for inherited diseases. Challenges for successful clinical development of molecular medicines include a better understanding of the natural histories of the diseases to be treated. For the specific case of autosomal dominant diseases causing blindness due to defects in the photoreceptors and the RPE, highly promising treatment strategies involving knockdown/replacement[20] and genome editing[46] must contend with the variation in disease expression ranging from nonpenetrance or slow progression to severe early disease.[47,48] The current work provides a quantitative framework for the natural history of structural and functional deficits across L-ORD retinas caused by a single founder variant in preparation for deciding optimal disease stages and retinal locations and evaluating the efficacy for molecular interventions that aim to achieve a permanent treatment for this blinding condition.

Photoreceptor Degeneration

End-stage disease in L-ORD corresponds to complete atrophy of photoreceptors and RPE that can extend across the whole retina and cause severe blindness in the eighth and ninth decades of life.[49] The first four decades of life are thought to be associated with normal photoreceptor structure and function. Complex spatiotemporal progression must occur after age 40, but informative long-term serial studies are rare. Earliest ophthalmoscopically visible retinal changes consisting of fine yellow–white punctate lesions have been observed within a C-shaped region encompassing paramacular to midperipheral eccentricities superior, temporal, or inferior to the fovea.[1,25] Limited serial data support the hypothesis that photoreceptor and RPE disease expand peripherally and centrally from the initial lesions.[25] To quantify the progression, we took a cross-sectional approach by evaluating 25 patients across varied ages and by sampling outer retinal structure across macular and extramacular retina up to midperipheral eccentricities. We used a delayed exponential equation[36–41] to model the data as an ensemble. The critical age at which photoreceptor degeneration started varied across the retina, with the temporal regions showing the earliest loss of ONL thickness consistent with previous clinical observations.[1,15,25,27] Unexpectedly, the start of inferior extramacular retinal degeneration was delayed by up to 12 years compared to equivalent eccentricity in the superior retina. Although superior–inferior asymmetry of disease progression has previously been observed in other retinal degenerations,[50–53] it is typically the inferior retina that shows greater/earlier disease, speculated to be driven by environmental light exposure over a lifetime.[54] Histopathological observations of normal-appearing far inferior retina in end-stage disease[1] could have been related to the current findings in macular and midperipheral retina at much earlier ages. At this time, it remains unclear what could contribute to the "inverted altitudinal" pattern observed in L-ORD, but intraretinal protein expression gradients relevant to the primary RPE disease[55] can be hypothesized.

When photoreceptor degeneration had initiated at each locus, progression in L-ORD across the retina followed a common trajectory, with an average rate of −0.045 $\log_{10}$/y (9.8%/y). We are aware of only two other retinal degenerative conditions analyzed with similar methods. In autosomal dominant retinitis pigmentosa caused by class B mutations in *rhodopsin*, the progression rate can be −0.03 $\log_{10}$/y (7%/y),[47] whereas in Leber congenital amaurosis (LCA) caused by mutations in *RPE65*, progression is −0.04 $\log_{10}$/y (8.8%/y).[56] Comparability between the progression rate in a late-onset disease such as L-ORD and in earlier onset diseases such as *RPE65*-LCA, irrespective of molecular cause, supports the hypothesis that a delayed exponential model can explain photoreceptor degeneration to a first approximation. Similar exponential progression rates (despite major differences in age of disease initiation) could implicate underlying programmed cell death mechanisms, working in a gene-agnostic fashion but involving disease- and location-specific delays. Then, after a watershed moment is reached at the critical age, stochastic effects result in predictable rate of cell death.[39,40]

L-ORD is thought to spare the fovea.[1,57] The simplest explanation for such an observation would involve hypothesizing that the rate of degeneration of foveal cones is much slower than the rate of degeneration in extrafoveal photoreceptors. However, our quantitative model of natural history supports an alternative. Specifically, our analyses show that it is the initiation of degeneration that is delayed at the fovea by about a decade compared to the rest of the macula; when initiated, degeneration at the fovea progresses at a rate comparable to the rest of the retina.

Outer Segments and SubRetinal Deposits

In most inherited retinal degenerations, shortening of the OS in areas with partial degeneration of photoreceptors is a common feature observed on histology in eye donors.[58] Why the OS shortens in still-surviving photoreceptors remains unclear, but changes in mitochondrial metabolism may be involved.[59] Imaging studies have shown that shortening of OS tends to be proportional to colocalized thinning of the ONL,[52,60–62] consistent with a previous study in an animal model of retinal degeneration.[63] Current work adds L-ORD to retinal diseases where proportional shortening of OS and thinning of the ONL have been demonstrated. It is important to note, however, that difficulties in differentiating the hyperscattering signal originating from OS tips and from sRET-Ds likely contributed to the substantial variability observed. We detected OCT signatures of sRET-Ds at some retinal locations in many eyes consistent with the previous literature on L-ORD.[17,25–28] Approaching the critical age at which photoreceptor degeneration starts, the prevalence of sRET-Ds tended to increase in L-ORD, which would be consistent with increased risk of photoreceptor atrophy caused by subretinal drusenoid deposits in AMD.[64] The unexpected exception in our cohort was the lack of any sRET-Ds detectable at any of the foveas during the decades preceding the critical age or following it. This implies involvement of rod photoreceptors in sRET-D formation.

Sub-RPE Deposits

One of the key features of L-ORD is a thick retina-wide deposit located between the basal lamina of the RPE and the inner collagenous layer of Bruch's membrane. These deposits appear to resemble the basal linear deposits found in AMD,[65] but histological evaluation of eye donors known to carry the c.489C>G variant in *C1QTNF5* has been limited. Specifically, the histology of family members of current patients P002, P003, and P006 has been previously published.[1,3,24] In addition, a study published in the pre-molecular era is now known to have included the c.489C>G founder variant (two eye donors[23] were from family L3, later clarified molecularly[3]). In contrast, the histopathology[66] in a family with a clinical diagnosis of L-ORD is now known to have been caused by a mutation in a gene that is different than *C1QTNF5*.

All molecularly confirmed histopathological studies of the c.489C>G variant[1,3,23,24] have been performed in older eye donors with complete photoreceptor atrophy and severe stage of disease. Therefore, the natural history of the initial formation of the sRPE-Ds and their spatial distribution and progression over the first seven decades of life remained unclear until the current work using non-invasive imaging studies. We are aware of only two previous studies that quantified the sRPE-D thickness,[4,67] and neither study evaluated young patients or mapped the inferred natural history of this key disease feature across a major section of the retina. Our results support the hypothesis that a sRPE-D > 10 µm thick is already formed diffusely across wide expanses of the retina at age 33 and later. Furthermore, additional data, limited to the macula in two subjects in their late 20s, suggest that no major change in deposition occurs between the late second decade and third decade of life, consistent with the slow expansion of sRPE-D thickness at an average rate of 2.7 µm per decade during the third and fourth decades of life. A constant, but slow, accumulation rate during these early time points would suggest that sRPE-D formation starts within the first decade of life, or even congenitally. This is surprising for a disease that does not manifest, clinically, for another four or five decades. Other diseases with thick sRPE-D formation, such as those caused by *TIMP3*[68] and *EFEMP1*[69] mutations, appear to show substantially later onset of sRPE-D formation[67] compared to L-ORD.

Up to critical ages, sRPE-D thickness appears to grow continuously. When photoreceptor degeneration starts, however, the sub-RPE growth rate flattens, and, a decade after critical age, there is evidence for clearance of sRPE-Ds in some retinal locations and continued accumulation in others. These findings likely imply that sRPE-Ds may be driven by an imbalance of accumulation and clearance of substances requiring photoreceptors. If supported by independent evidence, we can infer that efficacious gene-based treatments for L-ORD could result in clearing of the sRPE-Ds over time.

Visual Function

Localized loss of a subset of photoreceptors and shortening of the OS in surviving photoreceptors should result in reduced quantum catch and thus correspond to loss of local light sensitivity. These effects were clear in the current cohort, which demonstrated major losses of rod and cone sensitivity after critical age. What was unexpected was increasingly greater losses in rod sensitivity starting two decades before critical age in extrafoveal locations and the loss of cone sensitivity starting a decade before critical age in the fovea. Lack of normal light sensitivity at locations with normal ONL thickness and normal OS length have important implications regarding the potential of L-ORD for treatment. A dissociation between retinal structure and visual function is a prerequisite for vision improvement with gene-correcting therapies.[70] In some retinal diseases, there is a relative dissociation, with a mismatch between the extent of photoreceptor degeneration and the magnitude of visual dysfunction,[45,47,71] whereas in others the dissociation is absolute, where normal retinal structure is matched to large loss of sensitivity.[72] Our current work shows that L-ORD encompasses both scenarios ranging from absolute to relative dissociation.

Treatment Strategy With Gene Editing

Gene-based therapies can arrest progressive cell loss and improve function in inherited diseases. Some of the best examples of success for gene-based therapies to date have occurred in recessively inherited retinal diseases with adeno-associated virus (AAV) vectored gene augmentation therapy.[73–75] For dominantly inherited retinal diseases, gene editing promises to be a permanent treatment.[46] Recent developments in gene-editing approaches have evolved CRISPR/Cas[76] gene editing, which is most effective for gene disruption as error-prone nonhomologous end joining predominates over low-efficiency homology-directed repair. None of the pathogenic variants identified in L-ORD[6,10–12] to date is a target for cytidine deaminase (C:G base pairs converted to T:A base pairs)[77] editing. Only one (P188L) could be targeted by adenosine deaminase (A:T converted to G:C) base editing,[78] and few are suitable targets for C:G to G:C base editors.[79–81]

In contrast to base editing, prime editing can install or correct any of the 12 possible transition and transversion

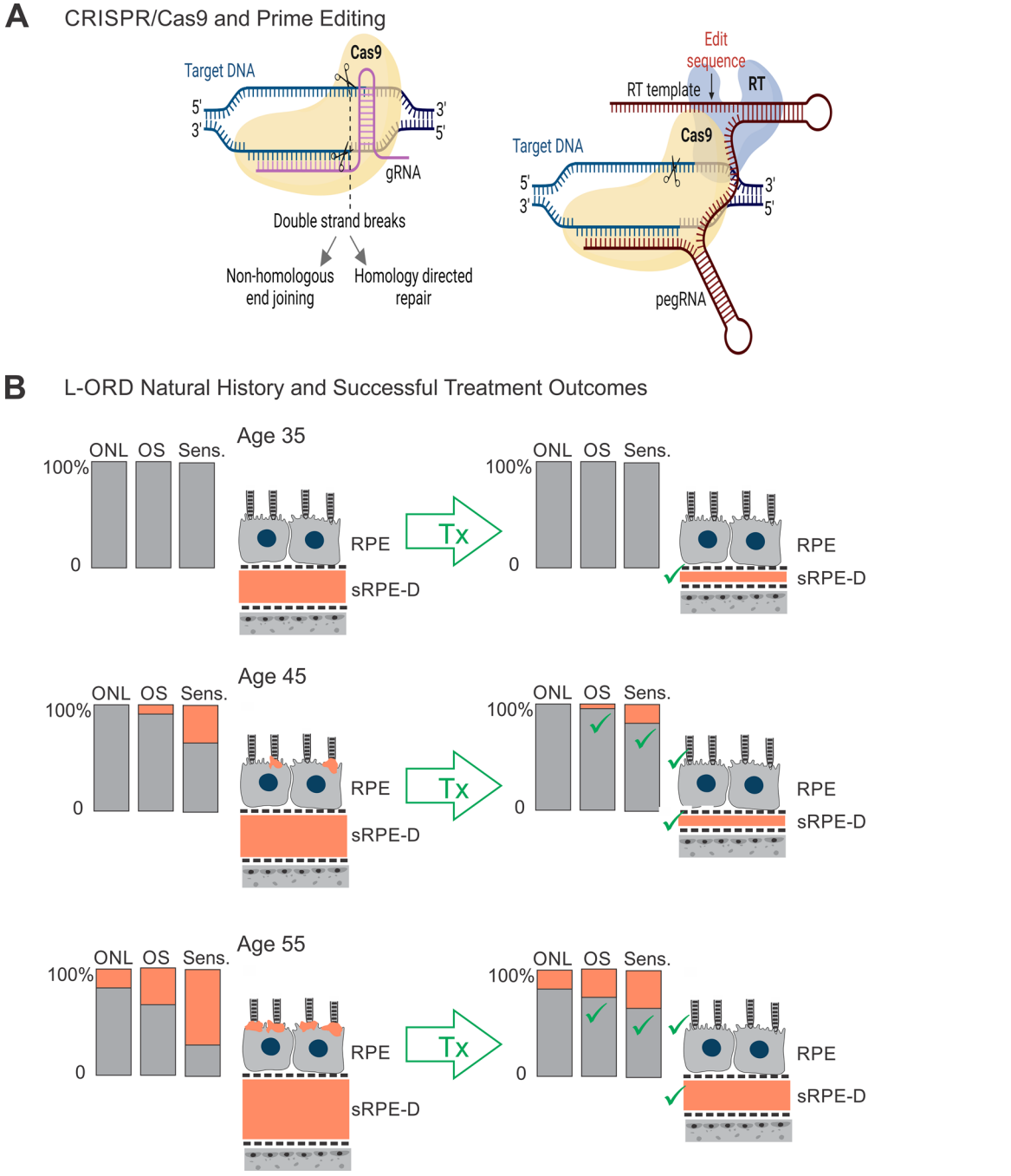

Figure 5. Targeting L-ORD with gene editing and predicted treatment outcomes at different disease stages. (**A**) The heterozygous c.489C>G variant in *C1QTNF5* creates a novel protospacer adjacent motif (PAM) site to which the Cas9 (*left*) or prime editor (*right*) enzymes can be targeted using specific guide RNA (gRNA or pegRNA). CRISPR/Cas9 gene editing to target the novel PAM site, resulting in double-strand breaks in DNA and enabling either nonhomologous end joining (indels) or homology-directed repair (with provision of a repair template). Prime editing offers a more precise method of gene editing, using Cas9 nickase to generate targeted single strand breaks before a tethered reverse transcriptase (RT) incorporates specific edits encoded by a repair template included in the pegRNA. (**B**) Schematic representation of L-ORD disease stages at 6° superior to the fovea. *Orange highlights* represent abnormal structural and functional features. *Green checks* represent successful outcomes expected at different stages.

base changes, as well as indels.[82] The prime editor (PE), comprised of SpCas9 nickase fused to an engineered reverse transcriptase, is programmed with a prime editing guide RNA (pegRNA) to both specify the target site and encode the required edit.[82] Recent work[83] to enhance the Cas9 nuclease and reverse transcriptase activity of prime editing enzymes, to improve pegRNA stability and nuclear localization of editing enzymes, and to increase the efficiency of DNA repair processes makes this versatile tool for programmable gene editing a specific and precise option of interest for future therapy for L-ORD. Notably, the heterozygous c.489C>G transversion variant in *C1QTNF5* creates a

novel protospacer adjacent motif (PAM) to which the Cas9[76] or PE[82] enzymes can be targeted using specific guide RNAs (Fig. 5A).

PE has shown promise for gene correction in mouse models of inherited retinal disease, targeting pathogenic variants in the DNA of RPE and photoreceptors.[84] Packaging constraints of viral vectors and concerns about long-term expression of editing machinery mean that challenges remain in the delivery of the bulky PE to target cells, including RPE. The benefits of this approach—minimal off-target editing, permanent correction of the pathogenic variant, and maintenance of endogenous gene expression levels—offer an exciting possibility in the development of future therapy for L-ORD.

In preparation for gene-editing trials, the current work aimed to provide quantitative phenomaps of structural and functional deficits caused by the heterozygous c.489C>G founder variant in *C1QTNF5*. We found that there are likely reversible abnormalities in all stages of disease as schematized by data collected at a location 6° superior to the fovea across all L-ORD retinas (Fig. 5B). At this location, 14 years before the critical age of 49 years, the only detectable abnormality would be a sRPE-D that could be expected to thin upon successful gene editing extrapolating from the apparent reversibility of these deposits at end-stage disease. By age 45 years, there would be some minor reduction of OS length, disproportionally larger deficits of sensitivity and sRET-Ds, and thicker sRPE-Ds. All four of these deficits would be expected to be ameliorated upon successful gene editing. By age 55 years, there would be progression of all previous deficits, as well as photoreceptor cell loss associated with thinning of the ONL layer. Successful gene editing would be expected to provide improvements for all deficits except for the loss of photoreceptors. With the estimation of the retinal variation of critical ages, our work lays a path for understanding which retinal locations are ideal candidates for interventions for L-ORD patients across a very wide range of ages.

Acknowledgments

Supported by LifeArc, Samuel G. Jacobson, MD, PhD, Memorial Fund, and an unrestricted grant from Research to Prevent Blindness.

Disclosure: **R.T.H. Li**, None; **A.J. Roman**, None; **A. Sumaroka**, None; **C.M. Stanton**, None; **M. Swider**, None; **A.V. Garafalo**, None; **E. Heon**, None; **A. Vincent**, None; **A.F. Wright**, None; **R. Megaw**, None; **T.S. Aleman**, None; **A.C. Browning**, None; **B. Dhillon**, None; **A.V. Cideciyan**, None

References

1. Kuntz CA, Jacobson SG, Cideciyan AV, et al. Sub-retinal pigment epithelial deposits in a dominant late-onset retinal degeneration. *Invest Ophthalmol Vis Sci*. 1996;37(9):1772–1782.
2. Jacobson SG, Cideciyan AV, Wright E, Wright AF. Phenotypic marker for early disease detection in dominant late-onset retinal degeneration. *Invest Ophthalmol Vis Sci*. 2001;42(8):1882–1890.
3. Hayward C, Shu X, Cideciyan AV, et al. Mutation in a short-chain collagen gene, *CTRP5*, results in extracellular deposit formation in late-onset retinal degenaration: a genetic model for age-related macular degeneration. *Hum Mol Genet*. 2003;12(20):2657–2667.
4. Jacobson SG, Cideciyan AV, Sumarok A, Roman AJ, Wright AF. Late-onset retinal degeneration caused by *C1QTNF5* mutation: sub-retinal pigment epithelium deposits and visual consequences. *JAMA Ophthalmol*. 2014;132:1252–1255.
5. Shu X, Tulloch B, Lennon A, et al. Biochemical characterisation of the *C1QTNF5* gene associated with late-onset retinal degeneration. A genetic model of age-related macular degeneration. *Adv Exp Med Biol*. 2005;572:41–48.
6. Stanton CM, Borooah S, Drake C, et al. Novel pathogenic mutations in C1QTNF5 support a dominant negative disease mechanism in late-onset retinal degeneration. *Sci Rep*. 2017;7(1):12147.
7. Mandal MN, Vasireddy V, Reddy GB, et al. CTRP5 is a membrane-associated and secretory protein in the RPE and ciliary body and the S163R mutation of CTRP5 impairs its secretion. *Invest Ophthalmol Vis Sci*. 2006;47(12):5505–5513.
8. Tu X, Palczewski K. Crystal structure of the globular domain of C1QTNF5: implications for late-onset retinal macular degeneration. *J Struct Biol*. 2012;180(3):439–446.
9. Tu X, Palczewski K. The macular degeneration-linked C1QTNF5 (S163) mutation causes higher-order structural rearrangements. *J Struct Biol*. 2014;186(1):86–94.
10. Borooah S, Stanton CM, Marsh J, et al. Whole genome sequencing reveals novel mutations causing autosomal dominant inherited macular degeneration. *Ophthalmic Genet*. 2018;39(6):763–770.
11. Rodriguez-Munoz A, Aller E, Jaijo T, et al. Expanding the clinical and molecular heterogeneity of nonsyndromic inherited retinal dystrophies. *J Mol Diagn*. 2020;22(4):532–543.
12. De Zaeytijd J, Coppieters F, De Bruyne M, et al. Longitudinal phenotypic study of late-onset retinal degeneration due to a founder variant c.562C>A p.(Pro188Thr) in the *C1QTNF5* gene. *Ophthalmic Genet*. 2021;42(5):521–532.
13. Kellner U, Weisschuh N, Weinitz S, et al. Autosomal dominant gyrate atrophy-like choroidal dystrophy revisited: 45 years follow-up and association with a novel *C1QTNF5* missense variant. *Int J Mol Sci*. 2021;22(4):2089.
14. Ayyagari R, Mandal MN, Karoukis AJ, et al. Late-onset macular degeneration and long anterior lens zonules result from a *CTRP5* gene mutation. *Invest Ophthalmol Vis Sci*. 2005;46(9):3363–3371.
15. Vincent A, Munier FL, Vandenhoven CC, et al. The characterization of retinal phenotype in a family with *C1QTNF5*-related late-onset retinal degeneration. *Retina*. 2012;32(8):1643–1651.
16. Papastavrou VT, Bradshaw KR, Aye KH, et al. Improvement of retinal function in L-ORD after prolonged dark adaptation. *Can J Ophthalmol*. 2015;50(2):112–118.
17. Papastavrou VT, O'Brien JM, Regan AJ, et al. The progression of macular structural and functional changes in late-onset retinal degeneration. *Retin Cases Brief Rep*. 2022;16(6):714–720.
18. Borooah S, Collins C, Wright A, Dhillon B. Late-onset retinal macular degeneration: clinical insights into an inherited retinal degeneration. *Br J Ophthalmol*. 2009;93(3):284–289.
19. Miyagishima KJ, Sharma R, Nimmagadda M, et al. AMPK modulation ameliorates dominant disease phenotypes of *CTRP5* variant in retinal degeneration. *Commun Biol*. 2021;4(1):1360.
20. Cideciyan AV, Sudharsan R, Dufour VL, et al. Mutation-independent rhodopsin gene therapy by knockdown and replacement with a single AAV vector. *Proc Natl Acad Sci USA*. 2018;115(36):E8547–E8556.
21. Diakatou M, Manes G, Bocquet B, et al. Genome editing as a treatment for the most prevalent causative genes

Investigative Ophthalmology & Visual Science

of autosomal dominant retinitis pigmentosa. *Int J Mol Sci*. 2019;20(10):2542.

22. Vandenberghe LH, Bell P, Maguire AM, et al. Dosage thresholds for AAV2 and AAV8 photoreceptor gene therapy in monkey. *Sci Transl Med*. 2011;3(88):88ra54.
23. Duvall J, McKechnie NM, Lee WR, et al. Extensive subretinal pigment epithelial deposit in two brothers suffering from dominant retinitis pigmentosa. A histopathological study. *Graefes Arch Clin Exp Ophthalmol*. 1986;224(3):299–309.
24. Gupta N, Brown KE, Milam AH. Activated microglia in human retinitis pigmentosa, late-onset retinal degeneration, and age-related macular degeneration. *Exp Eye Res*. 2003;76(4):463–471.
25. Cukras C, Flamendorf J, Wong WT, et al. Longitudinal structural changes in late-onset retinal degeneration. *Retina*. 2016;36(12):2348–2356.
26. Borooah S, Papastavrou V, Lando L, et al. Reticular pseudodrusen in late-onset retinal degeneration. *Ophthalmol Retina*. 2021;5(10):1043–1051.
27. Vanderford EK, De Silva T, Noriega D, et al. Quantitative analysis of longitudinal changes in multimodal imaging of late-onset retinal degeneration. *Retina*. 2021;41(8):1701–1708.
28. Oncel D, Corradetti G, Sadda SR. Extensive temporal subretinal drusenoid deposits as an early manifestation of late-onset retinal degeneration. *Can J Ophthalmol*. 2023;58(5):e225–e228.
29. Cideciyan AV, Hufnagel RB, Carroll J, et al. Human cone visual pigment deletions spare sufficient photoreceptors to warrant gene therapy. *Hum Gene Ther*. 2013;24(12):993–1006.
30. Cideciyan AV, Krishnan AK, Roman AJ, et al. Measures of function and structure to determine phenotypic features, natural history, and treatment outcomes in inherited retinal diseases. *Annu Rev Vis Sci*. 2021;7(1):747–772.
31. Lujan BJ, Roorda A, Knighton RW, Carroll J. Revealing Henle's fiber layer using spectral domain optical coherence tomography. *Invest Ophthalmol Vis Sci*. 2011;52(3):1486–1492.
32. Jacobson SG, Voigt WJ, Parel JM, et al. Automated light- and dark-adapted perimetry for evaluating retinitis pigmentosa. *Ophthalmology*. 1986;93(12):1604–1611.
33. Roman AJ, Powers CA, Semenov EP, et al. Short-wavelength sensitive cone (S-cone) testing as an outcome measure for *NR2E3* clinical treatment trials. *Int J Mol Sci*. 2019;20(10):2497.
34. Simunovic MP, Hess K, Avery N, Mammo Z. Threshold versus intensity functions in two-colour automated perimetry. *Ophthalmic Physiol Opt*. 2021;41:157–164.
35. Simunovic MP, Hess K, Gillies MC. Impairments in cone pigment regeneration and absolute threshold in macular telangiectasia type 2. *Retina*. 2022;42(3):569–575.
36. Berson EL, Sandberg MA, Rosner B, et al. Natural course of retinitis pigmentosa over a three-year interval. *Am J Ophthalmol*. 1985;99(3):240–251.
37. Massof RW, Finkelstein D. A two-stage hypothesis for the natural course of retinitis pigmentosa. In: Zrenner E, Krastel H, Goebel HH, eds. *Research in Retinitis Pigmentosa Advances in the Biosciences*. Oxford: Pergamon Press; 1987.
38. Birch DG, Anderson JL, Fish GE. Yearly rates of rod and cone functional loss in retinitis pigmentosa and cone-rod dystrophy. *Ophthalmology*. 1999;106(2):258–268.
39. Clarke G, Collins RA, Leavitt BR, et al. A one-hit model of cell death in inherited neuronal degenerations. *Nature*. 2000;406(6792):195–199.
40. Clarke G, Lumsden CJ. Heterogeneous cellular environments modulate one-hit neuronal death kinetics. *Brain Res Bull*. 2005;65(1):59–67.
41. Cideciyan AV, Swider M, Aleman TS, et al. ABCA4 disease progression and a proposed strategy for gene therapy. *Hum Mol Genet*. 2009;18(5):931–941.
42. Byrd RH, Lu PH, Nocedal J, Zhu CY. A limited memory algorithm for bound constrained optimization. *SIAM J Sci Comput*. 1995;16(5):1190–1208.
43. Nash JC. On best practice optimization methods in R. *J Stat Softw*. 2014;60(2):1–14.
44. Cideciyan AV, Jacobson SG, Sumaroka A, et al. Photoreceptor function and structure in retinal degenerations caused by biallelic *BEST1* mutations. *Vision Res*. 2023;203:108157.
45. Jacobson SG, Aleman TS, Cideciyan AV, et al. Identifying photoreceptors in blind eyes caused by *RPE65* mutations: prerequisite for human gene therapy success. *Proc Natl Acad Sci USA*. 2005;102(17):6177–6182.
46. Yan AL, Du SW, Palczewski K. Genome editing, a superior therapy for inherited retinal diseases. *Vision Res*. 2023;206:108192.
47. Cideciyan AV, Jacobson SG, Roman AJ, et al. Rod function deficit in retained photoreceptors of patients with class B *Rhodopsin* mutations. *Sci Rep*. 2020;10(1):12552.
48. Wheway G, Douglas A, Baralle D, Guillot E. Mutation spectrum of *PRPF31*, genotype-phenotype correlation in retinitis pigmentosa, and opportunities for therapy. *Exp Eye Res*. 2020;192:107950.
49. Lando L, Borooah S. Late-onset retinal degeneration: clinical perspectives. *Clin Ophthalmol*. 2022;16:3225–3246.
50. Cideciyan AV, Hood DC, Huang Y, et al. Disease sequence from mutant rhodopsin allele to rod and cone photoreceptor degeneration in man. *Proc Natl Acad Sci USA*. 1998;95(12):7103–7108.
51. Jacobson S, Aleman T, Sumaroka A, et al. Disease boundaries in the retina of patients with Usher syndrome caused by *MYO7A* gene mutations. *Invest Ophthalmol Vis Sci*. 2009;50(4):1886–1894.
52. Sumaroka A, Matsui R, Cideciyan AV, et al. Outer retinal changes including the ellipsoid zone band in Usher syndrome 1B due to *MYO7A* mutations. *Invest Ophthalmol Vis Sci*. 2016;57(9):OCT253–OCT261.
53. Sumaroka A, Cideciyan AV, Charng J, et al. Autosomal dominant retinitis pigmentosa due to class B *Rhodopsin* mutations: an objective outcome for future treatment trials. *Int J Mol Sci*. 2019;20(21):5344.
54. Cideciyan AV, Jacobson SG, Aleman TS, et al. In vivo dynamics of retinal injury and repair in the rhodopsin mutant dog model of human retinitis pigmentosa. *Proc Natl Acad Sci USA*. 2005;102(14):5233–5238.
55. Ortolan D, Sharma R, Volkov A, et al. Single-cell-resolution map of human retinal pigment epithelium helps discover subpopulations with differential disease sensitivity. *Proc Natl Acad Sci USA*. 2022;119(19):e2117553119.
56. Cideciyan AV, Jacobson SG, Beltran WA, et al. Human retinal gene therapy for Leber congenital amaurosis shows advancing retinal degeneration despite enduring visual improvement. *Proc Natl Acad Sci USA*. 2013;110(6):E517–E525.
57. Borooah S, Papastavrou VT, Lando L, et al. Characterizing the natural history of foveal-sparing atrophic late-onset retinal degeneration. *Retina*. 2021;41(6):1329–1337.
58. Milam AH, Li ZY, Fariss RN. Histopathology of the human retina in retinitis pigmentosa. *Prog Retin Eye Res*. 1998;17(2):175–205.
59. Todorova V, Stauffacher MF, Ravotto L, et al. Deficits in mitochondrial TCA cycle and OXPHOS precede rod photoreceptor degeneration during chronic HIF activation. *Mol Neurodegener*. 2023;18(1):15.
60. Sadigh S, Cideciyan AV, Sumaroka A, et al. Abnormal thickening as well as thinning of the photoreceptor layer in intermediate age-related macular degeneration. *Invest Ophthalmol Vis Sci*. 2013;54(3):1603–1612.

Investigative Ophthalmology & Visual Science

61. Sadigh S, Luo X, Cideciyan AV, et al. Drusen and photoreceptor abnormalities in African-Americans with intermediate non-neovascular age-related macular degeneration. *Curr Eye Res*. 2015;40(4):398–406.
62. Jacobson SG, McGuigan DB, Sumaroka A, et al. Complexity of the class B phenotype in autosomal dominant retinitis pigmentosa due to rhodopsin mutations. *Invest Ophthalmol Vis Sci*. 2016;57(11):4847–4858.
63. Machida S, Kondo M, Jamison JA, et al. P23H rhodopsin transgenic rat: correlation of retinal function with histopathology. *Invest Ophthalmol Vis Sci*. 2000;41(10):3200–3209.
64. Spaide RF, Ooto S, Curcio CA. Subretinal drusenoid deposits AKA pseudodrusen. *Surv Ophthalmol*. 2018;63(6):782–815.
65. Hammadi S, Tzoumas N, Ferrara M, et al. Bruch's membrane: a key consideration with complement-based therapies for age-related macular degeneration. *J Clin Med*. 2023;12(8):2870.
66. Milam AH, Curcio CA, Cideciyan AV, et al. Dominant late-onset retinal degeneration with regional variation of sub-retinal pigment epithelium deposits, retinal function, and photoreceptor degeneration. *Ophthalmology*. 2000;107(12):2256–2266.
67. Khan KN, Borooah S, Lando L, et al. Quantifying the separation between the retinal pigment epithelium and Bruch's membrane using optical coherence tomography in patients with inherited macular degeneration. *Transl Vis Sci Technol*. 2020;9(6):26.
68. Weber BH, Vogt G, Pruett RC, et al. Mutations in the tissue inhibitor of metalloproteinases-3 (TIMP3) in patients with Sorsby's fundus dystrophy. *Nat Genet*. 1994;8(4):352–356.
69. Stone EM, Lotery AJ, Munier FL, et al. A single EFEMP1 mutation associated with both Malattia Leventinese and Doyne honeycomb retinal dystrophy. *Nat Genet*. 1999;22(2):199–202.
70. Cideciyan AV, Jacobson SG. Leber congenital amaurosis (LCA): potential for improvement of vision. *Invest Ophthalmol Vis Sci*. 2019;60(5):1680–1695.
71. Sumaroka A, Garafalo AV, Semenov EP, et al. Treatment potential for macular cone vision in Leber congenital amaurosis due to *CEP290* or *NPHP5* mutations: predictions from artificial intelligence. *Invest Ophthalmol Vis Sci*. 2019;60(7):2551–2562.
72. Stunkel ML, Brodie SE, Cideciyan AV, et al. Expanded retinal disease spectrum associated with autosomal recessive mutations in *GUCY2D*. *Am J Ophthalmol*. 2018;190:58–68.
73. Acland GM, Aguirre GD, Ray J, et al. Gene therapy restores vision in a canine model of childhood blindness. *Nat Genet*. 2001;28(1):92–95.
74. Cideciyan AV, Aleman TS, Boye SL, et al. Human gene therapy for RPE65 isomerase deficiency activates the retinoid cycle of vision but with slow rod kinetics. *Proc Natl Acad Sci USA*. 2008;105(39):15112–15117.
75. Jacobson SG, Cideciyan AV, Ho AC, et al. Night vision restored in days after decades of congenital blindness. *iScience*. 2022;25(10):105274.
76. Doudna JA, Charpentier E. Genome editing. The new frontier of genome engineering with CRISPR-Cas9. *Science*. 2014;346(6213):1258096.
77. Komor AC, Kim YB, Packer MS, et al. Programmable editing of a target base in genomic DNA without double-stranded DNA cleavage. *Nature*. 2016;533(7603):420–424.
78. Gaudelli NM, Komor AC, Rees HA, et al. Programmable base editing of A*T to G*C in genomic DNA without DNA cleavage. *Nature*. 2017;551(7681):464–471.
79. Kurt IC, Zhou R, Iyer S, et al. CRISPR C-to-G base editors for inducing targeted DNA transversions in human cells. *Nat Biotechnol*. 2021;39(1):41–46.
80. Zhao D, Li J, Li S, et al. Glycosylase base editors enable C-to-A and C-to-G base changes. *Nat Biotechnol*. 2021;39(1):35–40.
81. Chen L, Park JE, Paa P, et al. Programmable C:G to G:C genome editing with CRISPR-Cas9-directed base excision repair proteins. *Nat Commun*. 2021;12(1):1384.
82. Anzalone AV, Randolph PB, Davis JR, et al. Search-and-replace genome editing without double-strand breaks or donor DNA. *Nature*. 2019;576(7785):149–157.
83. Chen PJ, Liu DR. Prime editing for precise and highly versatile genome manipulation. *Nat Rev Genet*. 2023;24(3):161–177.
84. Jang H, Jo DH, Cho CS, et al. Application of prime editing to the correction of mutations and phenotypes in adult mice with liver and eye diseases. *Nat Biomed Eng*. 2022;6(2):181–194.

Investigative Ophthalmology & Visual Science